Dynamical structures in binary media of potassium-driven neurons

D. E. Postnov,[1] F. Müller,[2] R. B. Schuppner,[2] and L. Schimansky-Geier[2]
[1]*Department of Physics, Saratov State University, Astrakhanskaya ul. 83, Saratov 410012, Russia*
[2]*Institute of Physics, Humboldt University of Berlin, Newtonstr. 15, D-12489 Berlin, Germany*
(Received 18 May 2009; revised manuscript received 3 August 2009; published 30 September 2009)

According to the conventional approach neural ensembles are modeled with fixed ionic concentrations in the extracellular environment. However, in some cases the extracellular concentration of potassium ions cannot be regarded as constant. Such cases represent specific chemical pathway for neurons to interact and can influence strongly the behavior of single neurons and of large ensembles. The released chemical agent diffuses in the external medium and lowers thresholds of individual excitable units. We address this problem by studying simplified excitable units given by a modified FitzHugh-Nagumo dynamics. In our model the neurons interact only chemically via the released and diffusing potassium in the surrounding nonactive medium and are permanently affected by noise. First, we study the dynamics of a single excitable unit embedded in the extracellular matter. That leads to a number of noise-induced effects such as self-modulation of firing rate in an individual neuron. After the consideration of two coupled neurons we consider the spatially extended situation. By holding parameters of the neuron fixed, various patterns appear ranging from spirals and traveling waves to oscillons and inverted structures depending on the parameters of the medium.

DOI: 10.1103/PhysRevE.80.031921 PACS number(s): 87.19.L−, 05.40.−a, 89.75.Kd

I. INTRODUCTION

According to a conventional view on neuronal dynamics, the electrical activity of a cell is represented by depolarization of its membrane potential. It is well described by the famous Hodgkin-Huxley model [1] describing the dynamics of the different ion channels and the gating ions. But also simplified model systems using less number of variables and control parameters [2] are able to specify the many aspects of neuronal dynamics. Among them, the FitzHugh-Nagumo (FHN) model [3] with a few control parameters plays the role of popular paradigm for many excitable systems. Due to its simplicity it helps a lot that ideas, which have been developed in neuronal dynamics, can be transferred to related problems of other nonlinear dynamics [4].

But an inevitable assumption and simplification has been made for these prototypical neuron models in terms of ionic currents. For example, it was assumed that in spite of transmembrane currents, both extracellular and intracellular ionic concentrations remain unchanged during depolarizations. Such a simplification is natural and acceptable if one considers individual neurons or segments of an excitable medium during a sufficiently short course of firing.

However, in other cases it will be not realistic. For example, there is experimental evidence that extracellular concentration of potassium ions can vary significantly during the course of intensive neuronal firings [5,6]. The detailed modeling of what happens during the course of ischemia shows the strong increase in extracellular potassium concentration up to 80 mM [7–11]. The glial cells, surrounding and supporting neurons, activate the potassium pumping when its concentration rises considerably (more than twice in medical leech) [12]. This excessive elevation of potassium concentration is considered to be an important element of mechanism of epileptic seizure development [13,14]. As the relevant computational studies, early modeling attempts were focused mostly on mechanisms of extracellular potassium clearance and showed that pathways different from diffusion must be involved in this process [15–18]. More recent models addressed the detailed neuronal morphology [19,20] or the role of specific ion channels in formation of self-sustained bursting behavior [13,21]. It was also shown that the interplay between ion concentrations and neural activity can lead to self-sustained pathological neural activation even in the case of an isolated cell. The wider list of modeling issues on the topic was recently reviewed in [22].

While the effects of variable ionic concentration are embedded in the quantitative high-dimensional models, it is difficult to distinguish them from other aspects of system behavior. At the same time, the set of frequently used simplified models does not cover the problem, just not having the appropriate control parameters.

One of the authors addressed this problem in recent works [23,24], where the effects of potassium mediated coupling were investigated using the Hodgkin-Huxley type model of leech neurons. It was shown that such rather simplified but still quantitative model reproduces the main features of small ensembles of potassium-driven neurons.

However, to study the behavior of large networks by means of a quantitative model, one needs to reduce the number of control parameters that are difficult to estimate or are just unknown. The alternative way is to develop a simplified nondimensional model that can capture at a qualitative level the specific features of potassium-coupled neurons and allows one to build large networks using a reasonable set of control parameters.

In the present work we derive such a model in the form of an extended FHN system [3] with an additional equation describing the dynamics of extracellular potassium. Since our model inherits the key features of a FHN neuron, it is physically transparent and tractable and thus provides the better chance to learn more about nonlinear mechanisms governing the formation of spatiotemporal patterns in large networks. Furthermore, compared to leaky integrate and fire models (LIF) the FHN includes the reset mechanism of the

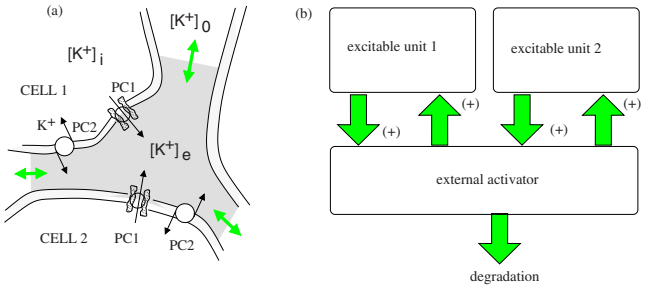

FIG. 1. (Color online) (a) Schematic representation of the potassium signaling pathways between closely located cells. (b) The corresponding structure of the functional model.

neuron. Some dynamical behavior which we will observe later on in the paper refers to the excited state of the FHN which is not provided by the LIF model [25,26].

Applied to interacting neurons we assume that the interaction of neurons is restricted to the single chemical pathway. Coupling takes place indirectly due to the potassium concentration outside the cells only. Although there is no explicit distance defined in the extended model, the neurons are strictly separated and a direct contact of the action potentials is excluded. Therefore, the transport of activity through the heterogeneous medium of neurons and exterior is slower than in a homogeneous excitable medium.

The patterns appearing in the two-dimensional system show phenomena, which are reminiscent of chemical experiments in which comparable heterogeneous situations such as two-layer systems or chemical oscillators moving in a diffusive environment, have been studied [27,28]. Also some of the presented structures relate to studies on the Ca^{2+} release across the endoplasmathic recituculum [29,30], where clusters with a finite number of ion channels on the recituculum take over the role of the noisy excitable neurons and Ca^{2+} diffuses freely in the cytoplasm.

In our work we attempt to classify the observed spatiotemporal patterns according to the relation between the key control parameters of the extracellular medium. The most noticeable behaviors are randomly walking spots, long-living meandering excitations, antiphase firing patterns, and inverted spirals and waves.

II. MINIMAL MODEL FOR A POTASSIUM-DRIVEN NEURON

A. Background

We consider an environment which is schematically depicted in Fig. 1(a). We assume that there is a certain volume between the cells from which the ionic exchange with the outer bath is rate limited. For simplicity we assume that this volume is homogeneous and we denote the potassium concentration here as $[K^+]_e$.

With time, particularly during firing events in neurons, the potassium channels PC1 in its membranes become open and outward currents from the cells deliver potassium to the extracellular space. Thus, $[K^+]_e$ rises while the intercellular potassium concentration $[K^+]_i$ decreases just slightly because $[K^+]_i \gg [K^+]_e$. In fact, one can neglect the associated intracellular changes in the potassium concentration and assume that this concentration remains constant.

Na-K ATP PC2 pumps K^+ back into the cells. This uptake is balanced by the leakage when the potassium concentration is at equilibrium value $[K^+]_0$. The exchange of K^+ ions with a surrounding bath is assumed to take place by a diffusion process, hence governed by the concentration difference between the exterior and the bath. Assuming the bath potassium concentration to be equal $[K^+]_0$, one can simplify the description of the process by incorporating all potassium uptake processes in an effective diffusion rate parameter γ.

Then the balance of potassium concentration in the intercellular space $[K^+]_e$ can be described as the following:

$$W\frac{d[K^+]_e}{dt} = \frac{1}{F}\sum_{i=1}^{N} I_{i,K} + \gamma([K^+]_0 - [K^+]_e), \tag{1}$$

where W is the extracellular volume per unit area of the membrane, N is the total number of cells being neighbors to this volume, and $I_{i,K}$ is the electric potassium current per unit area from the ith cell which is divided by Faraday's constant F to provide the ion flow. The second term $\gamma([K^+]_0 - [K^+]_e)$ describes the effective diffusion of potassium to and from the bath. This balance Eq. (1) provides the basis for the qualitative description in terms of a functional model we will introduce below.

Note that the variation in the ratio between the extra- and intracellular potassium concentrations affects the corresponding (Nernst) potential and, hence, the firing activity. The considerable rise of extracellular potassium concentration depolarizes the cell and can evoke the transition to spontaneous firing. However, too high extracellular potassium concentration becomes toxic and can block the cell activity completely.

B. Model

In this subsection we propose a functional model that aims the qualitative reproduction of main effects arising if a variable extracellular potassium concentration is taken into account. The structure of the model is schematically depicted in Fig. 1(b). Namely, several excitable units standing for a number of neurons contribute to the extracellular potassium increase. This "external activator" stands for the intercellular space between the cells with variable potassium concentration. It is (i) activated during a high-level state of one of the excitable units, (ii) provides an additional stimulus to the excitable units, and (iii) relaxes to an equilibrium when it receives no activation.

Let us first confine to a single neuron interacting with the external medium. Particularly, we will implement the activity of the excitable neuron by the FHN system [2,3]. Therefore, we assume that the gating of potassium release of a single neuron is given by

$$\varepsilon\dot{x} = x - x^3/3 - y, \tag{2}$$

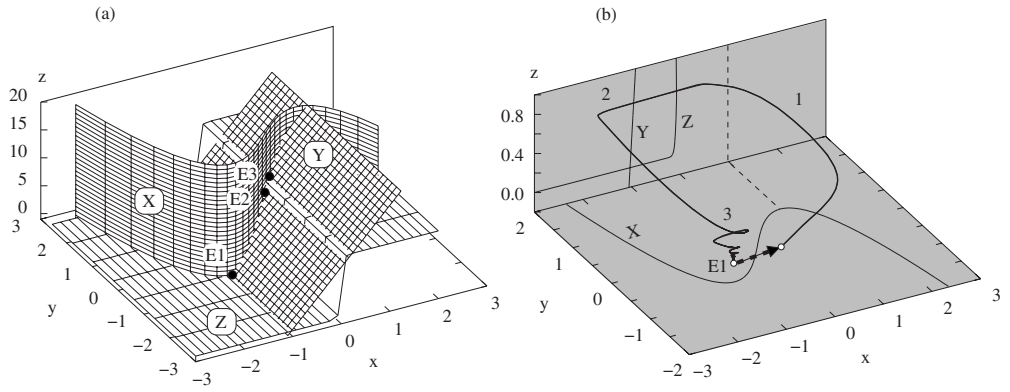

FIG. 2. (a) The three-dimensional plot of nullclines for the FHN-K model. The intersections of the cubic x nullcline, linear y nullcline, and sigmoidal-shaped z nullcline may provide three equilibrium points. (b) shows a representative trajectory near the stable equilibrium point E1 (thick line). The arrow indicates the initial perturbation.

$$\tau(x)\dot{y} = x + a - Cz, \tag{3}$$

where ε controls the time scale separation of the fast activator x and the slow inhibitor y. The operating regime of the FHN neuron is defined by a playing the role similar to the applied current in ionic current-based neuron models. We assume that it may fluctuate around some mean value a_0:

$$a = a_0 + \sqrt{2D}\xi(t), \tag{4}$$

where $\xi(t)$ is white Gaussian noise with zero mean and intensity is scaled by D.

An additional time scale $\tau(x)$ in Eq. (3) is introduced in order to control the two time scales, associated with firing (high level of x variable) and refractory state (low level of x) independently, which will gain importance in our problem. Specifically, we introduce the sigmoidal function

$$\Psi(x) = \frac{1}{2}\left[1 + \tanh\left(\frac{x}{x_s}\right)\right], \tag{5}$$

which is sensitive to the current value of the x variable: it tends to zero for $x \ll 0$, and to 1 if $x \gg 0$, while x_s scales the transition between these states. Actually, we use Eq. (5) as a smooth replacement of a Heaviside function to distinguish between the excited and the resting states of the FHN neuron. With Eq. (5) $\tau(x)$ shapes as

$$\tau(x) = \tau_l + (\tau_r - \tau_l)\Psi(x) \tag{6}$$

and takes values τ_l and τ_r in the rest and excited states, respectively.

We label the variable dimensionless extracellular potassium concentration by $z(t) \geq 0$. Its dynamics is given in accordance with Eq. (1) by

$$\dot{z} = \alpha g(x) - \beta z, \tag{7}$$

with $z = z^0 = 0$ corresponding to the steady concentration $[K^+]_0$ and β is the rate of ion losses. Respectively the parameter α stands for the summary ionic fluxes outward the cells. It scales inversely as well to the size of the extracellular volume. These fluxes are released into the exterior for high x values if the cell is excited and channels are open ($x \approx 2$). They disappear in the rest state $x \approx -1$ if channels are closed. Hence, likewise for the time scales we are able to use the function Eq. (5) as switcher in Eq. (7). Hence, we will set $g(x) = \Psi(x)$.

The value of z enters in Eq. (3) with a factor C. It represents the depolarizing effect of the increased extracellular concentration. For a given nonvanishing value of z it results in an additional shift of the y nullcline decreasing effectively the excitability value a. Mathematically we can call it a second activator which was previously introduced in models for nonlinear semiconductors [31].

The set of equations described above is dimensionless and, therefore, the relationship to ionic current-based neuronal models can be only qualitative. However, for the sake of simplicity and to keep the connection with the original problem, we will use the terminology from neurophysiology further on in order to describe the dynamic behavior of the model as well as the meaning of control parameters. In the following we refer to system (2)–(7) as the FHN-K model.

For the numerical simulations the following values of control parameter values were used: $\varepsilon = 0.04$, $a_0 = 1.04$, $C = 0.0 \ldots 0.1$, $\alpha = 1.0 \ldots 12.0$, $\beta = 0.05 \ldots 0.5$, $x_0 = 0.0$, $x_s = 0.2$, $\tau_l = 1.0 \ldots 10.0$, and $\tau_r = 1.0$. It sets the neuron without the regulation by external potassium ($C = 0$) in an excitable regime.

C. Nullclines and fixed points of the single-unit model

Let us look for the main features of the model in terms of the steady states and their stability. Note at $C = 0$ our model converges back to the original FitzHugh-Nagumo model with cubic and linear nullclines and one single equilibrium point, which is stable for $|a_0| > 1$ and unstable otherwise. Including the z dynamics the model [Eqs. (2)–(7)] possesses three nullcline surfaces, which are depicted in Fig. 2(a) and labeled X, Y, and Z according to the equation they satisfy. One can see that more than one intersection is possible. Namely, the condition $\dot{x} = \dot{y} = \dot{z} = 0$ gives for the steady-state values x^0:

$$x^0 + a_0 = \frac{1}{2}\frac{C\alpha}{\beta}\left[1 + \tanh\left(\frac{x^0}{x_s}\right)\right]. \tag{8}$$

We use a small x_s and the right-hand side of Eq. (8) becomes nearly a step function. Then one fixed point can be found

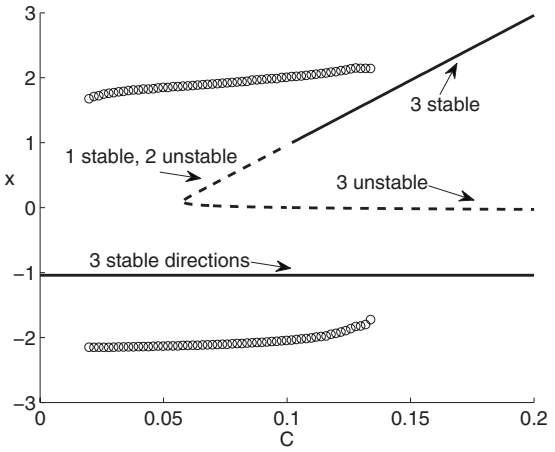

FIG. 3. Bifurcation diagram for C as the control parameter. The x value of the fixed points is plotted (dashed and solid lines). Circles correspond to the extremal elongation x values of the limit cycle.

$x_1^0 \approx -a_0$, which is always stable for the parameter range we will consider. Thus, the system needs overthreshold stimuli to enhance states with states $z > 0$.

Taking C as the control parameter regulating the coupling strength to the exterior variable z two additional fixed points bifurcate at a critical value C_{crit} resulting from

$$\eta C_{\text{crit}}\left(1 + \sqrt{1 - \frac{2x_s}{\eta C_{\text{crit}}}}\right) - x_s \,\text{atanh}\left(\sqrt{1 - \frac{2x_s}{\eta C_{\text{crit}}}}\right) - a = 0 \tag{9}$$

with $\eta = \frac{\alpha}{2\beta}$.

Sections of Eq. (9) are depicted in Fig. 3. The upper fixed point follows $x_3^0 = C\alpha/\beta - a_0$ and the corresponding z value is the highest z level the system can reach ($z_3^0 = z_{\max} = \alpha/\beta$). The fixed point in between is located at $x_2 \approx x_s(2\alpha\beta)/(\alpha C - 2\beta x s)$ which is only weakly dependent on C and is unstable in every direction. In Fig. 2(a) they are labeled with E1, E2, and E3, respectively.

In Fig. 2(b) a representative trajectory starting in the E1 vicinity is shown. The nullcline surfaces are given as projections on the horizontal and vertical planes. The arrow indicates the initial perturbation that kicks the phase point from E1. After a superthreshold push, the trajectory quickly moves rightward, then slowly moves along the y direction, but during this time it also moves upward approaching the z nullcline. The vertical component of movement is defined by α. This segment is labeled with 1. Within the segment 2 of the trajectory, the vertical component changes its direction; now it moves downward controlled by β. When the phase point comes back to the vicinity of the equilibrium point, it is still raised along the z axis. From this level, the phase point moves downward with pronounced damped oscillations. Besides the fixed points there is also a parameter range where a stable limit cycle appears (see the circles in Fig. 3 which indicate the extremal elongation in x for the stable periodic orbit). Initially started outside of the basin of attraction of the stable fixed points every trajectory ends up on that limit

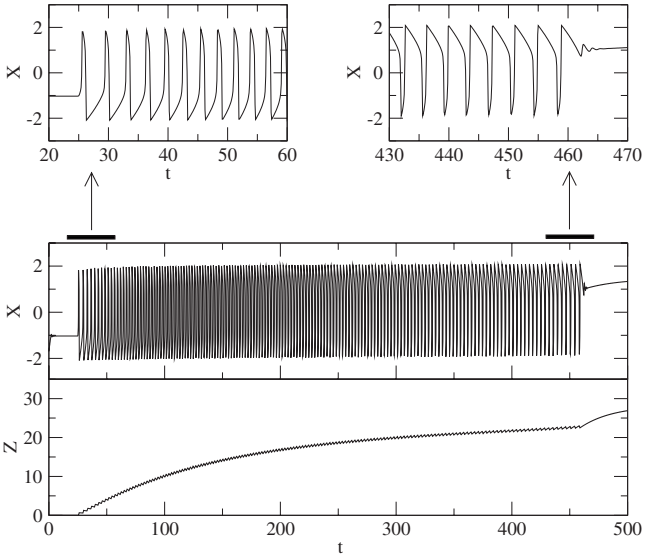

FIG. 4. Transition to the stable state at the activation state. After initiating the oscillation of x, the value of z rises and drives the system to the upper fixed point. In insets (top row) the corresponding change in the spikes for x is illustrated. (parameters: $\tau_l = \tau_r = 1$, $\beta = 0.0354 \ll \alpha = 1.0$)

cycle leading to an oscillatory behavior in x and y and a nearly constant level of z. Due to a saddle-node bifurcation the limit cycle loses stability in one direction for too small and too high values of C. The thereby created saddlelike limit cycle annihilates with the upper fixed point E3 via a Hopf bifurcation illustrated in Fig. 3 at the transition from the dashed to the solid line.

Beyond the limit cycle in a parameter range, where only the two stable fixed points exist, x and y also start to oscillate as a long-living transient when perturbating the lower fixed point initiation as depicted in Fig. 4. In that case the z level increases successively lifting the system up to the maximal value. Thus, the depolarizing spikes transform to polarization spikes elongating from the depolarized state down to the former resting polarized level. For the selected set of parameters the level of z still increases. The inverse firing process stops and reaches the stable steady state E3 where neurons are embedded in extracellular space contaminated by potassium.

III. NOISY BEHAVIOR OF A SINGLE UNIT

To understand the specific features of the FHN-K model in a noisy regime, let us first consider the segment 3 of the trajectory from Fig. 2(b) in terms of the excitation threshold. Figure 5(a) shows the time courses of the model variables at $a = 1.004$ when a short external pulse initiates the generation of a single spike. For specific values of α, the activation of z variable is relatively fast. In the middle panel of Fig. 5 one can compare the inhibitor behavior for $C = 0.008$ (solid curve) compared with the $C = 0$ case (dashed curve). Generally, the solid curve runs lower after the spike was generated. However, there is a more complex response near the resting state.

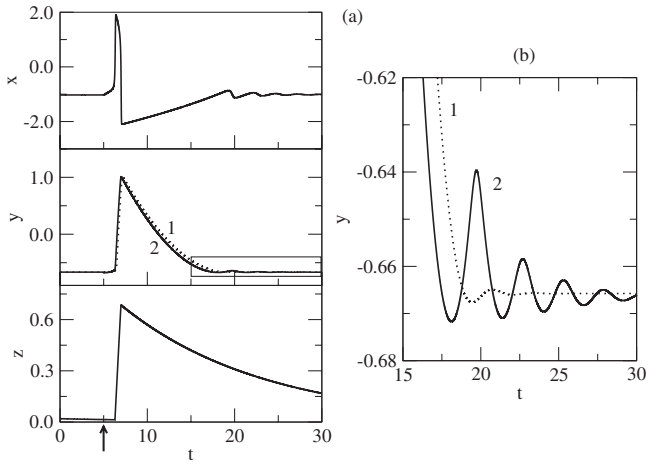

FIG. 5. (a) Temporal evolution after perturbation in the single-unit model at $C=0.008$. The spike is initiated by a short excitatory pulse at the time indicated by the black arrow. Dotted line (1) in the middle panel shows the y-time course for $C=0.0$. (b) The enlargement of rectangular area in (a) shows the subthreshold oscillations after spiking. The dotted (1) and solid (2) lines illustrate the cases of $C=0.0$ and $C=0.008$, respectively.

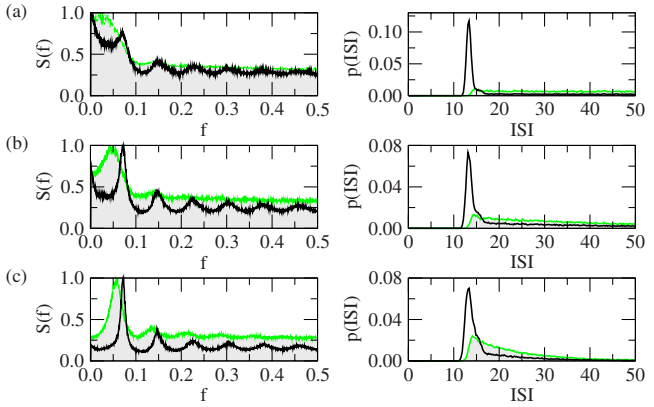

FIG. 6. (Color online) The spectral power density (left panels) and the probability distribution density of interspike intervals (right panels) for the single-unit model with noise. For comparison the maxima of the spectra are set to 1. Curves in black were obtained with $C=0.03$. Curves in gray with filled area were obtained with $C=0.0$ illustrating the behavior of the unperturbed FHN model. Noise intensity takes values $D=0.005$, $D=0.007$, and $D=0.01$ from top to bottom.

Figure 5(b) shows details. As we discussed above, an increased value of z evokes damped oscillations. During maxima of these oscillations the distance to values in phase space where a new excitation starts is minimal. Hence, during the moments of maximal elongation a weaker external forcing is sufficient to excite the next spike. This feature is important for understanding how noisy input acts in this model. Namely, after a spike was produced and the refractory time is over, there are few moments of larger probability for the next noise-induced firing. It resembles the behavior of so-called resonate-and-fire neurons [32,33] with subthreshold oscillations. But, differently, it occurs only after a spiking event, if still the exterior with $z\neq 0$ influences the behavior of the neuron.

The noisy behavior of model (2)–(6) is significantly controlled by the mechanism described above. For appropriate small D values a larger number of noise-induced spikes appears at the first elongation after approaching the rest state as shown at $t\approx 20$ in Fig. 5(b). There is a kind of stochastic positive feedback: once appeared, the noise-induced spiking can continue showing high regularity. If at this state current noise values were too small to override the minimized threshold, then the next spike will occur after a considerably longer time interval and noisy bursting is observed [33–35].

The described subthreshold oscillations are responsible for specific features of the averaged spectral power density $S(f)$. In the left column of Fig. 6 we compare the densities of the unperturbed FHN model (case $C=0$, given in gray) and of our model at $C=0.03$ [Eqs. (2)–(6)]. For all panels of the figure, the noise intensity D is assumed to be small, so the noisy forcing can be regarded as weak. Both cases start with just the same shape of $S(f)$, when only few spikes appear during the observation time (not shown in figure). In the FHN model, the further increasing of D leads to the formation of a broad peak at zero frequency that moves rightward and reaches the position at $f\approx 0.06$ at $D=0.01$. It corresponds to the quite regular firing due to the effect of coherence resonance [4,36,37]. Model (2)–(6) shows a similar power spectrum at very weak and at the final ($D=0.01$) noise strength, while the evolution of the spectra with increasing noise is different. Instead of a single broad peak at zero, two sharp peaks appear at zero and at $f\approx 0.075$. The inspection of time courses shows that the first peak corresponds to the randomly appeared bursts, while the second peak corresponds to the mean interspike distance within bursts. With increasing D, the peak at zero gradually disappears, while the peak at $f\approx 0.075$ collects more power. The third row of panels in Fig. 6 shows the considerably higher regularity of firing process in model (2)–(6) comparing with the FHN model. A similar effect can be observed by inspecting the probability distribution density of interspike intervals (ISI) as shown in the right column of Fig. 6. While the activity near zero frequency is mapped on interval values with larger than 20 time units, a pronounced peak is observed at ISI values ≈ 1 which grows up to an optimal value with increasing intensity of noise D.

To summarize, the noisy behavior of a single excitable unit is characterized by coherence resonance and by excitation of bursting with (statistically) large intervals between groups of spike. This interesting dynamics is reflected by both the spectral power density and the ISI distribution density. The origin of this feature is what one can call a subsequent self-induced depolarization in interaction with the exterior potassium. Note that this result is consistent with previously reported behavior of higher-dimensional quantitative models [19–21]

IV. TWO EXCITABLE UNITS INTERACTING WITH A COMMON EXTERIOR

The above described self-depolarization plays an important role when two excitable cells share one reservoir with

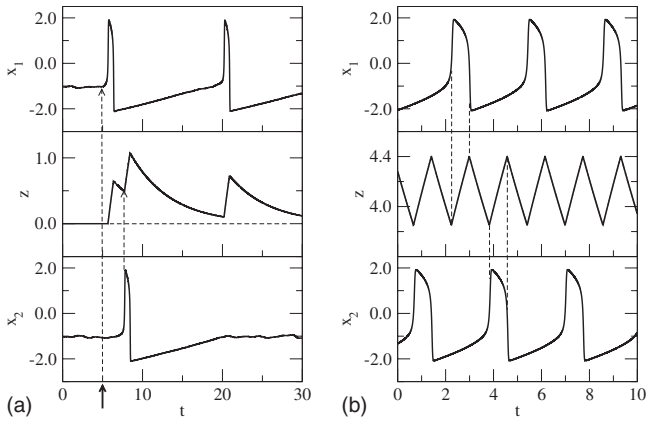

FIG. 7. Characteristic operating regimes of two coupled excitable units. Left panel: temporal evolution at weak noise. The first unit with x_1 starts firing first and provides an increase in the common external z level. It depolarizes the second unit and supports its noise-induced firing. Right panel: both units are in an oscillatory regime and show firing in antiphase. The frequency of the common output has doubled. The limit cycle of these oscillations is in coexistence with the stable fixed point E_1.

density $z(t)$. Therefore, Eq. (7) is replaced by

$$\dot{z} = \alpha[\Psi(x_1) + \Psi(x_2)] - \beta z, \tag{10}$$

where x_1 and x_2 belong to the first and second unit each described by equations like Eqs. (2) and (3) with the common variable $z(t)$.

In such a case, firing of one unit provides depolarization for both. Figure 7(a) illustrates the interaction. Originally, taking separately both units are excitable, so that without external input they remain in the rest position. When a noisy stimulus or an external perturbation initiates a spike in the first unit as shown in Fig. 7(a), almost instantaneously the second unit becomes strongly depolarized and starts also firing with large probability. Considering the collective response, it creates a doublet, like it is shown in Fig. 7(a) at $t \in (5,10)$. Note that the specific time interval in which the second spike appears depends on the current values of the noisy stimulus.

If the feedback controlled by C is strong enough, a self-sustained continuous firing occurs after one of the units was excited. In this regime in case of identical units equally spaced time intervals between spikes of the first and the second units are adjusted [Fig. 7(b)]. The two units fire perfectly in antiphase an effect which is known from glycolytic oscillations in cells [38].

Looking forward to the firing patterns in the 2D array of many units discussed in the next section, one can expect both: a temporal shifted firing of neighboring neurons ("one-induced-by-another" pattern) as well as a tendency to antiphase firing of neighboring units. The latter shows a doubled frequency in the collective response.

V. NOISY DYNAMICS OF SPATIALLY EXTENDED MODELS

Coming to the extended scenario we consider an inhomogeneous medium with separated active units on the one hand and exterior modeled by z on the other hand. There are two main possibilities to construct large ensembles of coupled units in two dimensions defined by Eqs. (2)–(6).

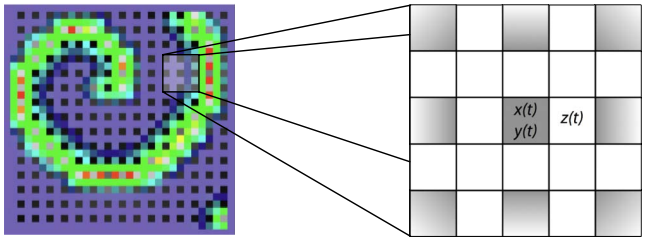

FIG. 8. (Color online) Schematic of the extended arrangement of neurons (N) and pure z cells in between.

On the one hand, on can assume that the $z(\vec{r},t)$ variable describes a continuous diffusive medium with spatial coordinates $\vec{r}=(r_1,r_2)$. The excitable units are placed in a second layer at locally separated sites coupled by the diffusing field $z(\vec{r},t)$. On the other hand, one can alternatively consider a binary medium, consisting of excitable elements embedded in the nonexcitable field $z(\vec{r},t)$, which diffuses in the remaining space of the two-dimensional medium.

The first approach is evidently and leads to a usual reaction-diffusion system with three variables. Two variables are locally defined and coupled via the third. One might imagine a two-layer system with excitable units located inside a gel with low connectivity. The interaction inside this first layer can be neglected compared to the diffusive coupling of the third species $z(\vec{r},t)$. For such mixed systems with densely packed excitable particles surrounded by reactive emulsions pattern formation has been observed in chemical experiments [39,40].

According to the original model of potassium mediated neuronal activity, the space is divided on cells that are electrochemical active surrounded of extracellular space being the diffusive medium for potassium ions. Thus, in the present work we will follow the second approach. However, we also considered the two-layer system, which we will compare to the binary system giving short remarks at the corresponding places.

In particular we use a regular array of active units in each row and column illustrated in Fig. 8 following Eqs. (2) and (3). For each point of the intermediate diffusive medium it holds:

$$\dot{z}_{ij} = \alpha \sum_{k \in nb_1} \Psi(x_k) + \gamma \sum_{l,m \in nb_2} (z_{lm} - z_{ij}) - \beta z_{ij}, \tag{11}$$

where the subscript ij denotes the current point in space. The second additional term describes the diffusion of the z field with the diffusion coefficient γ. The sum indices $nb_{1,2}$ denote the sets of neighboring "neurons" and coupled units, respectively. We have implemented several types of coupling such as nearest- or next-nearest neighbor coupling for nb_1 and/or nb_2. To keep it clear we discuss the results only for the coupling to the next eight surrounding boxes, where the diagonal elements are scaled by a factor of $1/\sqrt{2}$. Taking more neighboring cells into account has no mentionable impact. Note, that in contrast to conventional reaction-diffusion sys-

TABLE I. Values of the parameters of the exterior.

Parameters	α	β	γ	τ_l	D
Set No. 1	50.0	6.0	2.0	1.5	0.00005
Set No. 2	60.0	6.0	130	1.5	0.02
Set No. 3	6.0	0.35	4.0	1.5	0.0001
Set No. 4	10.0	0.6	0.2	2.0	0.00002
Set No. 5	150.0	6.3	2.0	1.5	0.003

tems, the active units do not interact mutually but only via the common variable z, whereas the exterior medium is locally coupled with itself and is additionally affected by the neurons activity.

One can expect that the interplay between the refractory time of an active cell (controlled by τ_l) and the time scale of extracellular space (defined by the parameters α, γ, and β in the equation for z) plays a key role in the spatiotemporal dynamics. Therefore, we have selected some representative examples that are discussed below as five trials.

All the computations are performed in conditions where the identical individual units possess at least one stable fixed point at $x^0=-a$, which we choose as the initial condition. The following parameters have been appointed in all cases: $\varepsilon=0.04$, $a_0=1.04$, $C=0.1$, $\tau_r=1.0$, $x_0=0$, and $x_s=0.05$. Essentially only the parameters of the exterior have been set to different values according to Table I.

With the increasing set number the mean z level rises successively corresponding to a growing value of the coupling parameter C. According to the bifurcation diagram (Fig. 3) we go to the right along the abscissa and encounter excitable, oscillatory, and bistable behavior. We underline that the rest state of the uncoupled FHN is always a stable homogeneous state of our dynamics with $z=0$. Excitations of spatiotemporal structures need overthreshold noisy stimuli or corresponding initial conditions.

A. Set No. 1: Waves, spots, and spirals (Fig. 9)

The local dynamics is excitable. By noise the units can be activated and release z to their neighborhood. In this case the outside concentration of the medium decays much faster than the units recover, while the diffusion is too slow to distribute the delivered z over a large distance. The units that crossed over in the refractory period ignite other neighboring units via the medium and a traveling noise-supported extended wave is excited as it is depicted in Fig. 9(a).

At the system borders or due to noise circular waves can break and the free endings curl to form a spiral wave. Although the dynamics is purely excitable at the chosen noise intensity waves appear very regularly, noticeable in the time series of Fig. 9(b). The mean firing rate of the active cells is $r_{mean}\approx 0.1$ and the mean exterior concentration is $z_{mean}\approx 0.8$.

The combination of the chosen diffusion $\gamma=2.0$ with considerable refractory time of neurons stabilizes the location of the center of noise-induced spiral wave in spite of all units receive random stimulus of the same intensity. One may eliminate in the dynamics the z variable which would reduce the system of equations to two components standing for a single activator x and inhibitor y. Compared to the usual case the coupling term (diffusion of activator) appears in the equation of the inhibitor similar to a Soret effect. Slightly increased noise strength destroys the spiral wave structure by splitting it into short fragmented traveling waves that nucleate and annihilate in a random manner.

The release of potassium in the exterior is still sufficiently low and so far no new fixed point bifurcates at high z values. Therefore, the background in the large refractory state relaxes always to small z values as indicated by the dominating dark color in the figure. In the two-layer system for a decay rate of $\beta\approx 4$ or smaller only short living wave segments supported by noise appear.

B. Set No. 2: Noise-supported traveling clusters (Fig. 10)

The pronounced difference to the former set of parameters is the very large z-diffusion coefficient γ and the high noise level. Nuclei that would lead to coherent patterns such as spirals diffuse very fast forming still connected clusters of delivered z. Such developed clusters can live relatively long wandering through the medium due to the noisy forcing.

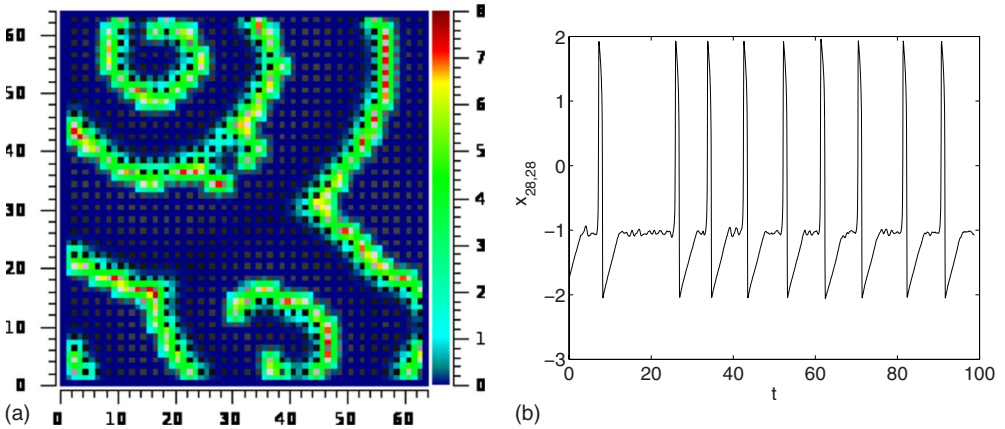

FIG. 9. (Color online) Parameter set no. 1: (a) noise-induced spirals and wave fronts. The color bar indicates the z level whereas white and black represent active cells in the excited and rest states, respectively. (b) Time series of an arbitrary chosen cell.

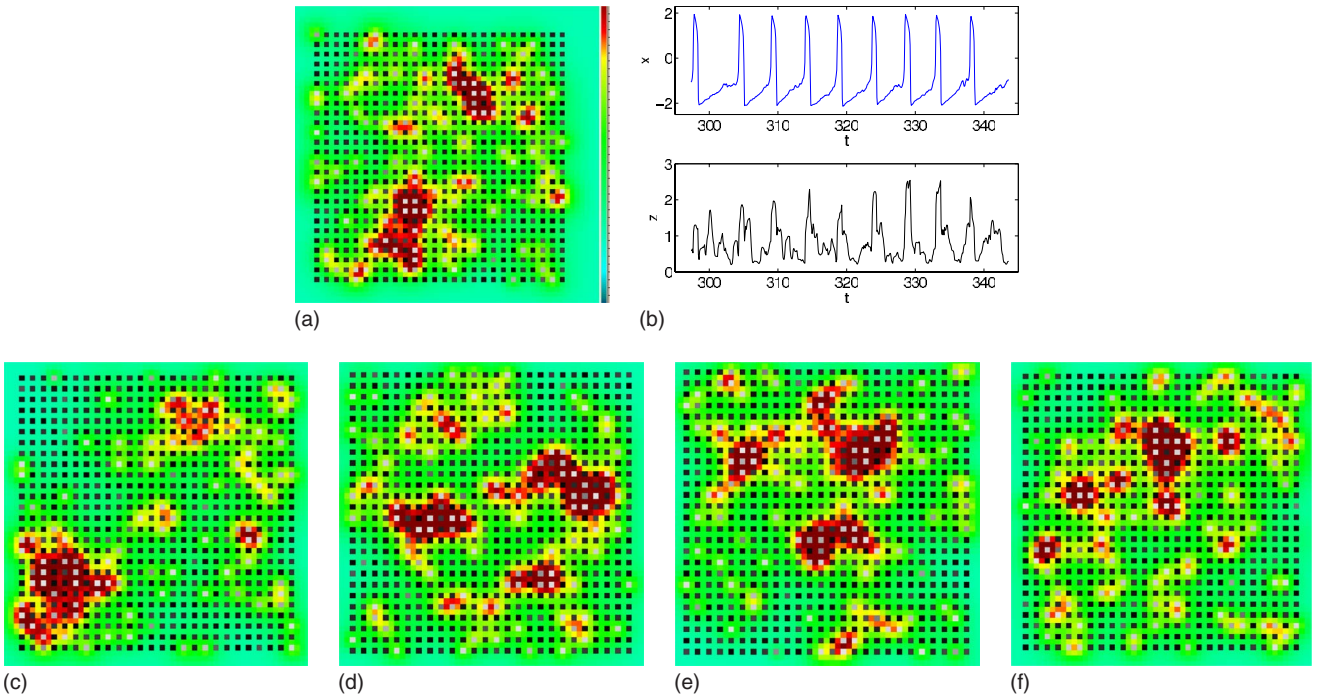

FIG. 10. (Color online) Parameter set no. 2: colors like in Fig. 9(a) self-feeding clusters. (b) Time series of an arbitrary chosen cell and of a neighboring z cell. (c)–(f) Snapshots of nucleating, wandering, and decaying clusters.

The local dynamics is excitable and possesses only the lower fixed point as a steady state. Due to the fast z diffusion a large vicinity of units gets activated whenever a unit is excited. It supports the formation of a localized high-level z region. Inside those areas the threshold of the units is lowered and the release of z increases. This process leads to self-feeding meandering cluster as depicted in the snapshots of Figs. 10(c)–10(f).

Note that noise is necessary over the whole time to keep the clusters alive. Switching the noise off leads to a complete decay of the z level to zero. For the given noise intensity the stochastically occurring spikes events are quite regular. The z level follows the activation and forms also coherent oscillationlike elongation as shown in Fig. 10(b). The mean rate is $r_{mean} \approx 0.2$ and the mean z concentration is $z_{mean} \approx 1.0$.

C. Set No. 3: Desynchronized oscillators embedded in a z sea (Fig. 11)

Compared to the former case less potassium is released but it is also slower decaying. The refractory time is short $\tau_l = O(1)$ compared to the decay time β^{-1} and therefore we observe oscillating units [Fig. 11(b)] embedded in a situation that high z values survive longer than the duration of one oscillation period. Thus, the exterior is permanently fed by potassium which is diffusing over long distances shown in Fig. 11(a).

Starting at the $z=0$ level, the active units first perform the noise-induced transition to the oscillatory behavior. Except for the initiating perturbation noise is not needed to keep the oscillation alive. All units move along the stable limit cycle but with different phases. Along such sites the medium is

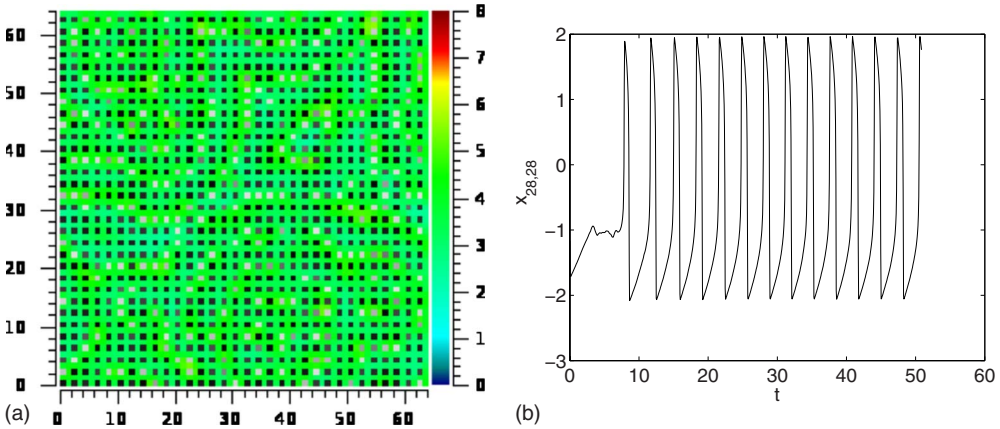

FIG. 11. (Color online) Parameter set no. 3: (a) elevated z level due to permanently oscillating active cells. Colors like in Fig. 9(a). (b) Time series of an arbitrary chosen cell.

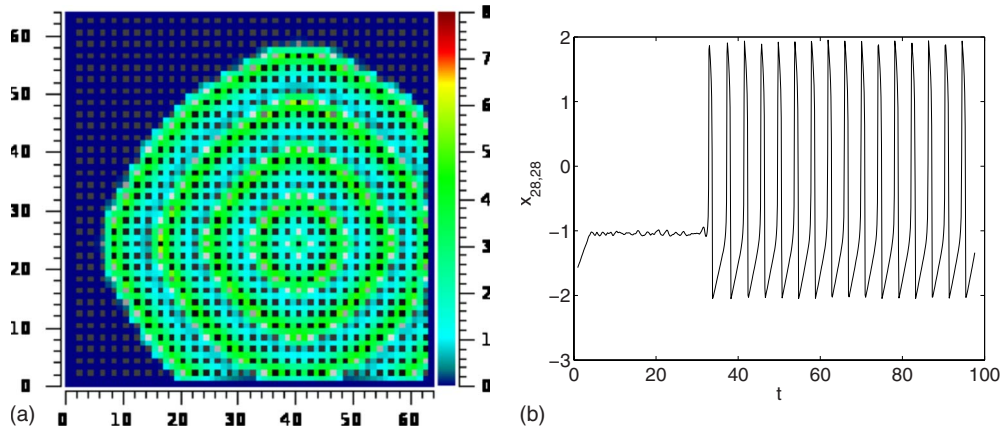

FIG. 12. (Color online) Parameter set no. 4: (a) noise-induced concentric waves. Colors like in Fig. 9(a). (b) Time series of an arbitrary chosen cell.

quickly filled with z which starts to propagate elevating the neighborhood and forming a frontlike spread over the space. It is a typical scenario of nucleation in systems with multiple attractors.

Despite that a second attractor at high z values exists it will never be reached due to the decay rate β which is still high enough to compensate the release of potassium with the rate α. Thus, a quasisteady picture remains with a sea of high potassium populated by active units blinking regularly and feeding the exterior with potassium. Here, we find for the oscillation frequency $r_{mean} \approx 0.34$ and for the mean exterior $z_{mean} \approx 5.7$.

Two times greater α and β and 20 times smaller diffusion originate another similar pattern: after some transient, high z concentration occupies all available space, after that, a noise-induced neuronal firing moving as complex pattern through the medium. A detailed inspection shows that the observed behavior is locally based on the antiphase firing of neighboring units inside the constant sea of high z level. In 2D space it produces a chesslike firing pattern, when all neighbors fire in antiphase. In the deterministic case it forms regular phase waves moving from borders to the center. Noise adds irregularity and evokes many additional patterns.

In Fig. 13(a) the spatial correlation function is shown for an arbitrary neuron over the distance to its neighboring excitable units along a row. The solid line represents the long-range correlation to the active units in the neighborhood, when the noise has not yet disturbed the wavelike propagation of the stimulus that lifts the units to the limit cycle.

A slow decay of the correlation is shown expressing the indirect diffusive coupling. The first dip corresponds to the next-nearest neuron which is less correlated with the considered unit than the next but one. It reflects that on average neighboring elements can fire preferable in antiphase.

However, a small amount of noise will drive the system to a complete desynchronized state after a couple of oscillations shown as the dashed line in Fig. 13(a). The described situation is typical for the studied extended system and can be found over a large parameter range. Also in the two-layer system the same oscillating regime exists for the same parameter set.

D. Set No. 4: Oscillations form a propagating ringlike pattern (Fig. 12)

Similar to the former parameter set, a single cell, fluctuating around the rest state, can reach the stable limit cycle, we mentioned above, by overcoming the unstable limit cycle due to noise. At this noise level those events are rare. Once happened β is so small that the z level around the oscillating cell can rise and reach the next cells without decaying before. Therefore, all active units can be elevated to the oscillatory behavior successively and a concentric wave appears shown in Fig. 12(a). A typical time series of x recorded from a single cell is depicted in Fig. 12(b). For the chosen parameters the oscillation period after the transition is $r_{mean} \approx 0.25$, while the z level averages $z_{mean} \approx 6.0$. Compared to the last case diffusion of potassium is reduced drastically. It gives reason that spatial structure can establish at length scale of a few neurons.

In Fig. 13(b) the spatial correlation is shown, where the solid line shows a long-range correlation shortly after initiating the wave pattern. The active units are well synchronized and it takes a longer time until the structure is destroyed by noise. This state corresponds to the dashed line in Fig. 13(b).

Increasing β the stable and unstable limit cycles annihilate and the local dynamics is excitable. A noise-induced superthreshold perturbation leads to a singular depolarization of the active cell and the z level in its neighborhood increases. Thus, the next cell becomes depolarized as well and a singular ringlike wave emerges.

Further increase in β allows only a small neighborhood of the initially activated cell to get enough released z. However, such activated wave segments can be stable a long time while traveling through the medium.

This kind of patterns always decays in the two-layer situation. The released z can diffuse to each site of the array without restriction. So the release rate α needs to be greater. For example, choosing $\alpha=15$ and a big enough initial nucleus an oscillon is formed. This structure is an extended but localized spot fed by oscillating cells inside and surrounded by inactive cells.

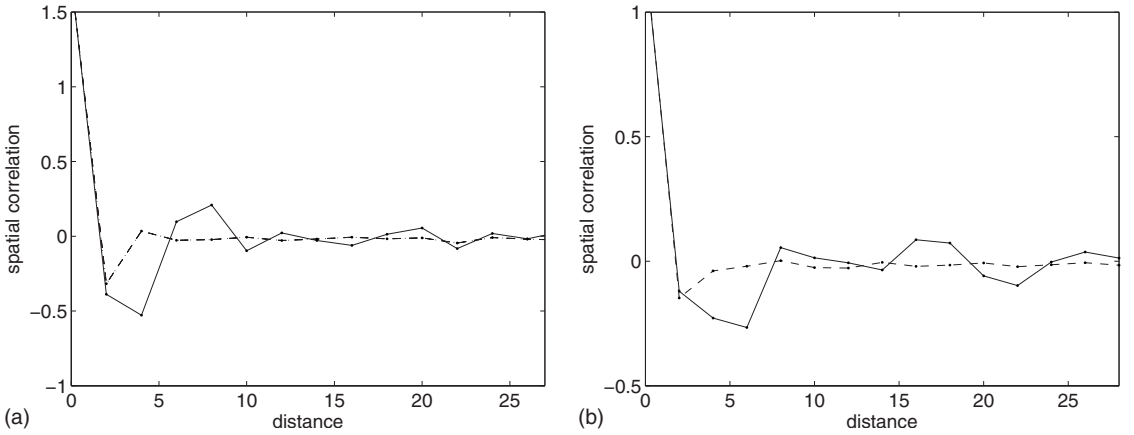

FIG. 13. The spatial correlations of set no. 3 (left) and set no. 4 (right) over the distance to neighboring neurons are shown without considering the inactive space. Solid lines indicate transient behavior for early times; dashed lines show the system which becomes uncorrelated due to noise.

E. Set No. 5: Bistability and inverted waves (Fig. 14)

Figure 14 illustrates the case of the highest release rate α considered here. After the nucleation of a bistable wave all the space becomes initially occupied by the high-level z state ($z=\alpha/\beta\approx 24$) which is stable due to the bifurcation of a second stable fixed point at the depolarized state of the cells. Thus, the vicinity of the activated cells is permanently filled with z dissipated with β and diffusively distributed with γ. An inverse situation occurs. Noise can create low level patterns such as inverted spirals or propagating waves shaped into the high-level z sea. They consist of polarized states which propagate through the medium. Such coherent patterns do not exist in the vicinity of the considered parameters for the two-layer system, after the high-level z state is reached. Only independent break-ins are taking place stochastically. Depending on the noise configuration it is also possible that the system reaches the $z=0$ state again by the appearance of the inverted bistable front.

Other types of unconventional patterns have been previously reported. These are rotating spirals or target waves which run from outward to the center called antispirals or antiwaves, respectively. Such patterns have been found in the Belousov-Zhabotinsky reaction and elsewhere and can be described by reaction-diffusion systems [41–43]. Note that in our case the rotational direction of the spirals and the propagation of the waves is the same as for common waves like presented in set no. 1.

From the dynamical point of view, the existence of this regime can be explained as follows. The considerable elevation of z shifts the operation point of core FHN model to the opposite side of the cubic nullcline. Operating on the background of high exterior z and corresponding to the shifted fixed point, each subthreshold perturbation leads to an inverted spike being the impulse from resting high level to the low one. Now τ_r controls the duration of a polarization spike while τ_l defines the refractory time [Fig. 14(b)] The above described mechanism is already discussed in Fig. 4 for a single active unit having two stable steady states.

VI. CONCLUSIONS

In this paper we have introduced a model that qualitatively describes the neuronal dynamics at variable extracel-

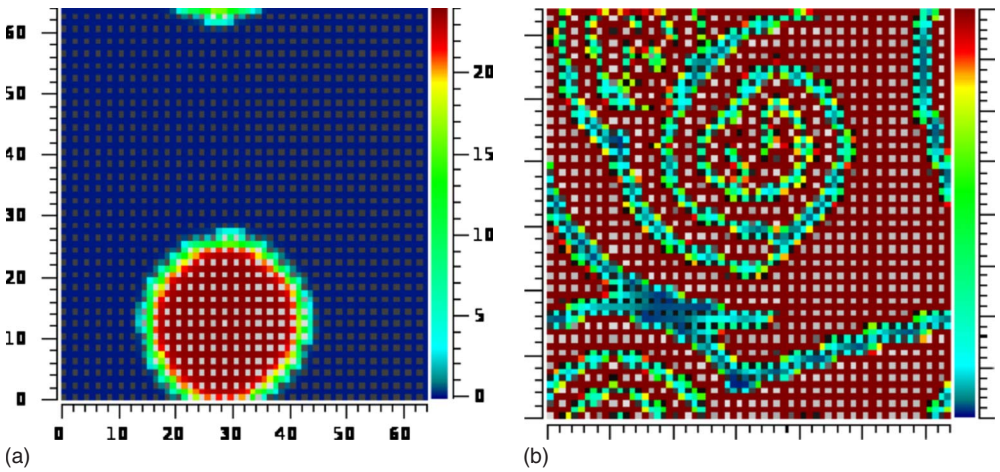

FIG. 14. (Color online) Parameter set no. 5: (a) a bistable wave covers the medium with the high-level z state. Colors like in Fig. 9(a). (b) Noise-induced inverted spirals and waves with polarized states appear. The scales are the same like in (a).

lular concentration of potassium ions. Using the FitzHugh-Nagumo model as prototype for an excitable unit, we added a pathway that qualitatively takes into account the potassium release from the neurons and the depolarization (threshold lowering) as a result of the increased extracellular potassium level.

The analyses of the model for a single unit, for two coupled units, as well as for an extended array have shown the following:

(i) The stochastic model of a potassium-driven excitable neuron exhibits bursting as the firing pattern. It is due to subthreshold oscillations for higher values of potassium. As a result, the power spectrum with increasing intensity differs from the typical one for an excitable system with strong time scale separation. It shows a pronounced and narrow peak at a frequency different from zero. The broad peak gradually close to zero frequency disappears with growing noise intensity.

(ii) In the excitable regime two potassium-coupled neurons being forced by noise show doublets of spikes. Firing of one neuron strongly depolarizes the second neuron and makes its firing almost inevitable. In many cases these doublets tend to an oscillatory behavior being synchronized in antiphase and possessing a frequency doubled to the spiking of a singular neuron.

(iii) A two-dimensional array of potassium-driven neurons shows a variety of noise-induced spatial-temporal firing patterns depending on the relation between the characteristic time scales of the model and the noise intensity. One of the most interesting patterns is the long-living randomly walking spots of depolarized states. Another effect is the high-level potassium state with inverted spirals of the polarized state being the result of the medium-driven shift of equilibrium state toward the right part of cubic nullcline.

In spite of simplicity of the generalized model we use, some links can be made between our results and relevant neurophysiological studies. Namely, the well known but still debating "potassium accumulation hypothesis" [22,44,45] considers the self-sustained rise of extracellular potassium as the cause of epileptiform activity. Taking it in mind, our computational results can be classified as the following: the short-term activation of z medium (including concentric and running waves) might describe the potassium dynamics within the physiological range, while the patterns with persistent high level of z variable resemble the formation of epileptic seizure and thus can be regarded as representing pathological conditions. Thus, an interesting future work can be done to reveal the possibility and conditions for mutual transitions between "normal" and "pathological" states.

ACKNOWLEDGMENTS

We thank S. Rüdiger (Berlin) for fruitful discussion and cooperation. D.P. acknowledges the support from RFBR Grant No. 09-02-01049. F.M. and L.S.G. acknowledge the support by the SFB 555 and R.B.S. and L.S.G. thank for support the Bernstein Center for Computational Neuroscience.

[1] A. L. Hodgkin and A. F. Huxley, J. Physiol. (London) **117**, 500 (1952).
[2] J. Keener and J. Sneyd, *Mathematical Physiology* (Springer, New York, 1998).
[3] R. A. FitzHugh, Biophys. J. **1**, 445 (1961).
[4] B. Lindner, J. Garcia-Ojalvo, A. B. Neiman, and L. Schimansky-Geier, Phys. Rep. **392**, 321 (2004).
[5] E. Sykova, Prog. Biophys. Mol. Biol. **42**, 135 (1983).
[6] Y. A. Dahlem, M. A. Dahlem, T. Mair, K. Braun, and S. C. Müller, Exp. Brain Res. **152**, 221 (2003).
[7] C.-S. Yi, A. L. Fogelson, J. P. Keener, and C. S. Peskin, J. Theor. Biol. **220**, 83 (2003).
[8] G. X. Yan, J. Chen, K. A. Yamada, A. G. Kleber, and P. G. Corr, J. Physiol. (London) **490**, 215 (1996).
[9] A. J. Hansen, Acta Physiol. Scand. **102**, 324 (1978).
[10] J. R. Cressman, Jr., G. Ullah, J. Ziburkus, S. J. Schiff, and E. Barreto, J. Comput. Neurosci. **26**, 159 (2009).
[11] G. Ullah, J. R. Cressman, E. Barreto, and S. J. Schiff, J. Comput. Neurosci. **26**, 171 (2009).
[12] J. W. Deitmer, C. R. Rose, T. Munsch, J. Schmidt, W. Nett, N.-P. Schneider, and C. Lohr, Glia **28**, 175 (1999).
[13] M. Bazhenov, I. Timofeev, M. Steriade, and T. J. Sejnowski, J. Neurophysiol. **92**, 1116 (2004).
[14] E.-H. Park and D. M. Durand, J. Theor. Biol. **238**, 666 (2006).
[15] B. A. Vern, W. H. Schuette, and L. E. Thibault, J. Neurophysiol. **40**, 1015 (1977).
[16] A. R. Gardner-Medwin, J. Physiol. (London) **335**, 393 (1983).
[17] L. L. Odette and E. A. Newman, Glia **1**, 198 (1988).
[18] I. Dietzel, U. Heinemann, and H. D. Lux, Glia **2**, 25 (1989).
[19] H. Kager, W. J. Wadman, and G. G. Somjen, J. Neurophysiol. **84**, 495 (2000).
[20] H. Kager, W. J. Wadman, and G. G. Somjen, J. Neurophysiol. **88**, 2700 (2002).
[21] F. Fröhlich, M. Bazhenov, I. Timofeev, M. Steriade, and T. J. Sejnowski, J. Neurosci. **26**, 6153 (2006).
[22] F. Fröhlich, M. Bazhenov, V. Iragui-Madoz, and T. J. Sejnowski, Neuroscientist **14**, 422 (2008).
[23] D. E. Postnov, L. S. Ryazanova, O. S. Sosnovtseva, and E. Mosekilde, Int. J. Neural Syst. **16**, 99 (2006).
[24] D. E. Postnov, L. S. Ryazanova, R. A. Zhirin, E. Mosekilde, and O. V. Sosnovtseva, Int. J. Neural Syst. **17**, 105 (2007).
[25] S. Coombes and Y. Timofeeva, Phys. Rev. E **68**, 021915 (2003).
[26] Y. Timofeeva, G. J. Lord, and S. Coombes, Neurocomputing **69**, 1058 (2006).
[27] I. Berenstein, M. Dolnik, L. Yang, A. M. Zhabotinsky, and I. R. Epstein, Phys. Rev. E **70**, 046219 (2004).
[28] A. F. Taylor, M. R. Tinsley, F. Wang, Z. Huang, and K. Showalter, Science **323**, 614 (2009).
[29] M. Falcke, New J. Phys. **5**, 96 (2003).
[30] J. W. Shuai and P. Jung, Phys. Rev. E **67**, 031905 (2003).
[31] C. Radehaus, R. Dohmen, H. Willebrand, and F.-J. Niedernos-

theide, Phys. Rev. A **42**, 7426 (1990).
[32] E. M. Izhikevich, Neural Networks **14**, 883 (2001).
[33] T. Verechtchaguina, L. Schimansky-Geier, and I. M. Sokolov, Phys. Rev. E **70**, 031916 (2004).
[34] T. Schwalger and L. Schimansky-Geier, Phys. Rev. E **77**, 031914 (2008).
[35] A. M. Lacasta, F. Saguès, and J. M. Sancho, Phys. Rev. E **66**, 045105(R) (2002).
[36] A. S. Pikovsky and J. Kurths, Phys. Rev. Lett. **78**, 775 (1997).
[37] S. K. Han, T. G. Yim, D. E. Postnov, and O. V. Sosnovtseva, Phys. Rev. Lett. **83**, 1771 (1999).
[38] J. Wolf and R. Heinrich, Biosystems **43**, 1 (1997).
[39] I. R. Epstein and V. K. Vanag, Chaos **15**, 047510 (2005).
[40] M. R. Tinsley, A. F. Taylor, Z. Huang, and K. Showalter, Phys. Rev. Lett. **102**, 158301 (2009).
[41] V. K. Vanag and I. R. Epstein, Science **294**, 835 (2001).
[42] X. Shao, Y. Wu, J. Zhang, H. Wang, and Q. Ouyang, Phys. Rev. Lett. **100**, 198304 (2008).
[43] E. M. Nicola, L. Brusch, and M. Bär, J. Phys. Chem. B **108**, 14733 (2004).
[44] J. D. Green, Physiol. Rev. **44**, 561 (1964).
[45] A. P. Fertziger and J. B. Ranck, Jr., Exp. Neurol. **26**, 571 (1970).